ARTICLE

doi:10.1038/nature10633

Neuronal filtering of multiplexed odour representations

Francisca Blumhagen[1]†*, Peixin Zhu[1]*, Jennifer Shum[1]†*, Yan-Ping Zhang Schärer[1]*, Emre Yaksi[2], Karl Deisseroth[3] & Rainer W. Friedrich[1,4]

Neuronal activity patterns contain information in their temporal structure, indicating that information transfer between neurons may be optimized by temporal filtering. In the zebrafish olfactory bulb, subsets of output neurons (mitral cells) engage in synchronized oscillations during odour responses, but information about odour identity is contained mostly in non-oscillatory firing rate patterns. Using optogenetic manipulations and odour stimulation, we found that firing rate responses of neurons in the posterior zone of the dorsal telencephalon (Dp), a target area homologous to olfactory cortex, were largely insensitive to oscillatory synchrony of mitral cells because passive membrane properties and synaptic currents act as low-pass filters. Nevertheless, synchrony influenced spike timing. Moreover, Dp neurons responded primarily during the decorrelated steady state of mitral cell activity patterns. Temporal filtering therefore tunes Dp neurons to components of mitral cell activity patterns that are particularly informative about precise odour identity. These results demonstrate how temporal filtering can extract specific information from multiplexed neuronal codes.

The temporal structure of neuronal activity patterns contains information that may be retrieved by temporal filtering operations[1–8]. Oscillatory synchronization has been implicated in sensory and cognitive processing based on the assumption that synchronization enhances the impact of neuronal ensembles on their targets[3,5,7,8]. Indeed, coincidence detection is a generic neuronal filtering operation that can be further supported by active conductances and synaptic microcircuits. However, few studies have directly demonstrated the impact of synchrony on neuronal responses in the intact brain[9–12]. Moreover, information can also be encoded by other temporal features of population activity patterns[6,13–20], and the information transmitted during a sensory response can change over time[20–24]. The retrieval of information from neuronal activity patterns thus depends on temporal filters that tune higher-order neurons to specific temporal structure in their input. Filtering is particularly important when different temporal features simultaneously transmit distinct messages (multiplexing)[13,15,24].

We explored temporal filtering during transformations of spatiotemporal activity patterns in the olfactory system of zebrafish. Odours stimulate combinations of mitral cells in the olfactory bulb, which project to multiple higher brain areas. In zebrafish, mitral cell activity patterns are dynamically reorganized during the initial phase of an odour response before they approach a steady state[5,22,24,25]. After approximately 400 ms, two important consequences of this reorganization emerge (Supplementary Fig. 1)[24]. First, odour-dependent subsets of mitral cells rhythmically synchronize their action potentials at a frequency near 20 Hz. Activity patterns across synchronized mitral cells are highly correlated in response to similar odours and contain information about molecular categories, but they are not well suited for precise odour identification. Second, patterns of non-synchronized spikes become decorrelated and informative about precise odour identity. Mitral cell activity patterns in the steady state therefore simultaneously convey information about complementary stimulus features[24]. Extracting information from these multiplexed activity patterns depends critically on temporal filtering by their targets. Precise odour identity could be efficiently decoded from late activity patterns across non-synchronized mitral cells, but this may be complicated by synchronized mitral cell ensembles as synchronization can have a strong impact on target neurons.

Optogenetic manipulation of synchrony

We first used an optogenetic approach to examine the impact of synchrony among mitral cells on neuronal responses in the posterior zone of the dorsal telencephalon (Dp), a major target of the olfactory bulb that is homologous to olfactory cortex[26,27]. In transgenic zebrafish expressing channelrhodopsin-2 (Chr2)[28,29] in sensory afferents[30], patterns of blue laser light were projected onto the ventral olfactory bulb using a digital micromirror device (DMD). Each of the $1{,}024 \times 768$ mirrors in the DMD was controlled independently with submillisecond temporal resolution. Light patterns consisted of distributed active squares ($50 \times 50\ \mu m^2$ or $20 \times 20\ \mu m^2$; Fig. 1a and Supplementary Fig. 2). Activation of individual squares near a mitral cell for 5 ms evoked depolarizations up to 10 mV and action potential firing (Supplementary Fig. 3). In a stimulus pattern, each mirror within an active square was switched on for 5 ms at a mean event rate of 20 Hz. Synchrony among pixels was then varied by periodically modulating the probability of events at a common carrier frequency of 20 Hz (Supplementary Fig. 4 and Supplementary Movies 1 and 2). Synchrony was quantified by a synchronization index, S, that ranges between zero (independent Poisson-distributed events) and infinity (perfectly synchronous events; Supplementary Fig. 4).

Mitral cells responded robustly to optical stimulation. As S was increased ($S = 0, 1, 10, \infty$), 20 Hz oscillatory fluctuations emerged in the membrane potential of individual neurons (Fig. 1a), as well as in averaged recordings (Fig. 1b–d; $n = 161$ responses of 49 mitral cells from 13 fish at each S; 3.4 ± 1.1 trials per stimulus; mean $\pm$ s.d.) and in the local field potential (LFP; Fig. 2 and Supplementary Fig. 5). The overall magnitude and time course of the mitral cell response,

[1]Friedrich Miescher Institute for Biomedical Research, Maulbeerstrasse 66, 4058 Basel, Switzerland. [2]Neuroelectronics Research Flanders, Kapeldreef 75, 3001 Leuven, Belgium. [3]Department of Bioengineering, Stanford University, Stanford, California 94305, USA. [4]University of Basel, 4003 Basel, Switzerland. †Present addresses: Novartis Pharma GmbH, 90327 Nuremberg, Germany (F.B.); Department of Neurology and Neurological Sciences, Stanford University, Stanford, California 94305, USA (J.S.).
*These authors contributed equally to this work.

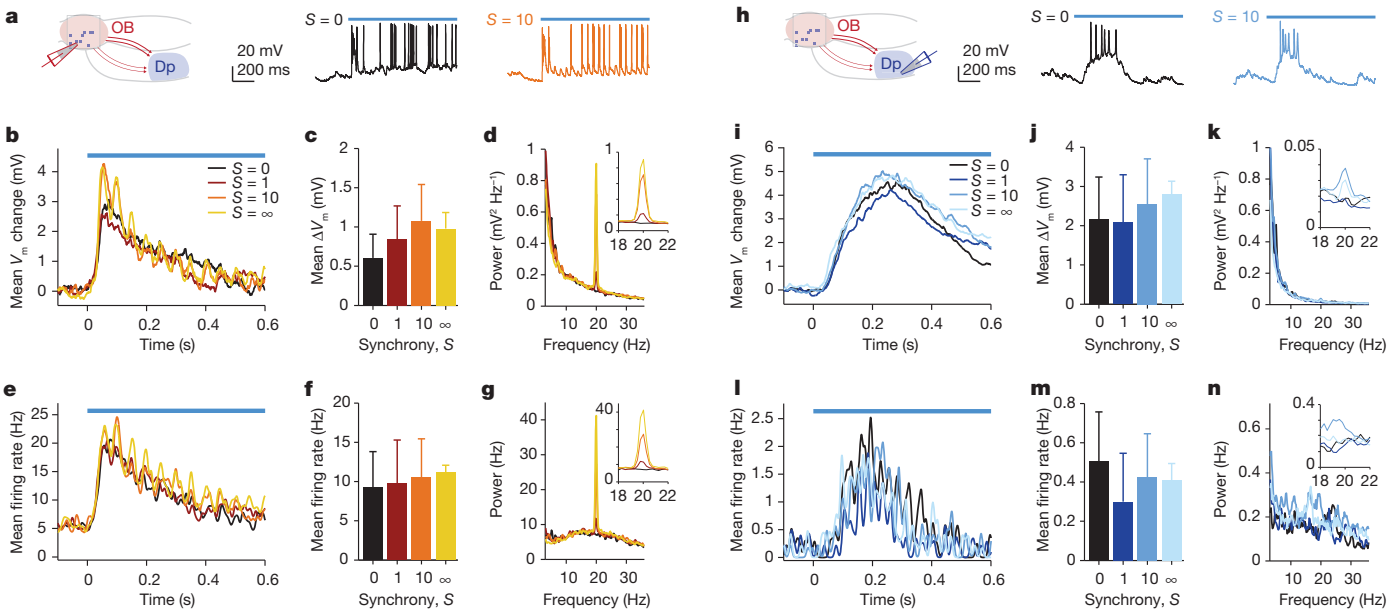

Figure 1 | Optogenetic manipulation of mitral cell synchrony and its effect on Dp neurons. **a**, Schematic illustration of optical stimulation in the olfactory bulb (OB) and responses of a mitral cell to the same spatial pattern at two different synchronies *S*. **b**, Mean membrane potential (V_m) response of mitral cells to the same optical stimulus patterns presented at four different synchronies *S* ($n = 161$ stimuli in 49 mitral cells at each *S*). Action potentials were removed before averaging by median filtering. **c**, Mean membrane potential change during the first second of optical stimulation as a function of synchrony. **d**, Power spectrum of the membrane potential, averaged over trials and neuron–stimulus pairs, during the first second of the response to optical stimulus patterns with different synchrony. Inset shows an enlargement around 20 Hz. **e**–**g**, Time course of mean mitral cell firing rate, mean mitral cell firing rate during the first second, and average power spectrum of mitral cell firing rate in response to patterns with different synchrony. Continuous firing rate traces were generated by convolving action potential events with a Gaussian kernel (s.d. = 5 ms). **h**–**n**, Same analysis for responses of Dp neurons. Error bars show s.d.

however, remained nearly constant (Fig. 1b, c). Similarly, increasing *S* strongly enhanced oscillatory synchronization of firing rate responses, with minimal effects on the magnitude and overall time course (Fig. 1e–g). Optical stimulation therefore allowed us to selectively modulate oscillatory synchrony among mitral cells.

We then stimulated the olfactory bulb with the same light patterns while recording from different types of Dp neurons (Fig. 1h and Supplementary Fig. 6). Dp neurons had low spontaneous activity (0.1 ± 0.5 Hz; mean ± s.d.) and usually responded to optical stimulation with a depolarization, but only a minority of responses were suprathreshold (77 out of 372 neuron–stimulus pairs; 21%). The mean membrane potential change and overall response time course were not substantially affected by synchrony (Fig. 1i, j; $n = 94$ responses of 34 Dp neurons from 10 fish at each *S*). Unlike in the olfactory bulb, increasing synchrony did not produce prominent oscillations in the membrane potential (Fig. 1h, i) or in the LFP measured in Dp (Fig. 2 and Supplementary Fig. 5). Even when depolarizations were large and when synchrony was high, oscillatory membrane potential fluctuations were small and occurred on top of a large, slow depolarization (Supplementary Fig. 7). Power spectral analysis revealed only a slight increase in membrane potential fluctuations at 20 Hz (Fig. 1k; note different scaling of inset). Action potential firing of Dp neurons did also not systematically depend on synchrony and showed no prominent 20 Hz oscillation at any level of synchronization (Fig. 1l–n). Moreover, switching synchrony from $S = 0$ to $S = \infty$ during optical stimulation failed to evoke an obvious response (Supplementary Fig. 8). Nevertheless, spikes evoked by oscillatory input occurred around a preferred phase of the LFP oscillation in the olfactory bulb (Supplementary Fig. 9). Oscillatory synchrony can therefore influence the timing of action potentials in Dp, but it did not increase the overall depolarization and firing rates.

Impact of synchrony on odour responses

To examine the impact of synchrony on odour responses of Dp neurons we performed whole-cell recordings during stimulation with natural odours (food extracts and amino acid odours; $n = 166$ neuron–odour

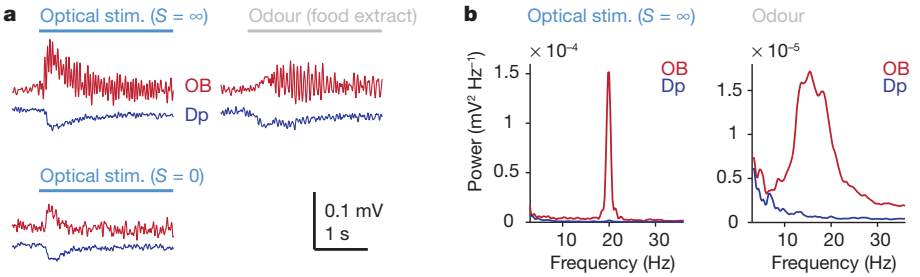

Figure 2 | Local field potential responses. **a**, Left: simultaneously recorded LFP responses in the olfactory bulb (OB; red) and Dp (blue) to optical stimulation with high synchrony ($S = \infty$; top) and no synchrony ($S = 0$; bottom). Right: LFP responses to odour stimulation (food extract; 5–40 Hz). **b**, Power spectra of LFP responses to optical stimulation with high synchrony (left; $S = \infty$) and odour stimulation (right) in the olfactory bulb (red) and in Dp (blue). Power spectra were calculated for each trial and averaged over trials and stimuli (olfactory bulb, odour: $n = 208$ stimuli in 17 fish; Dp, odour: $n = 20$ stimuli in 4 fish; olfactory bulb and Dp, optical: $n = 16$ stimuli in 4 fish).

pairs, 57 Dp neurons in 43 fish; mean number of repetitions per stimulus, 4.1 ± 1.8). As observed previously[26], responses of Dp neurons were often depolarizing, but many remained subthreshold (Supplementary Fig. 10). Power spectral analysis showed no evidence for oscillatory modulation of the membrane potential, spiking activity, or LFP in Dp during odour stimulation (Fig. 2 and Supplementary Fig. 5).

In 122 neuron–odour pairs (492 individual trials), we simultaneously recorded the LFP oscillation in the olfactory bulb and compared it to membrane potential fluctuations of Dp neurons in the same frequency band (5–40 Hz; Fig. 3a). In some cases, a weak oscillatory cross-correlation was observed (Supplementary Fig. 11); however, membrane potential fluctuations were substantially smaller than the slow depolarization. On average, the amplitude of membrane potential fluctuations (filtered 5 – 40 Hz) was 0.7 ± 0.7 mV (mean ± s.d.; mean maximal fluctuations, 2.4 ± 1.9 mV). In the same neurons, the mean difference between the resting potential and action potential threshold was 27.7 ± 5.9 mV (Fig. 3b). The amplitude of the slow depolarization had a mean of 15.4 ± 12.7 mV (± s.d.) and varied substantially across neurons and odours (Fig. 3b). Spike output therefore depended primarily on the magnitude of the slow depolarization, rather than on oscillatory fluctuations. Nevertheless, spikes of Dp neurons occurred around a preferred phase of the LFP oscillation in the olfactory bulb (Supplementary Fig. 9), indicating that oscillatory synchronization influenced action potential timing.

To confirm further that oscillatory fluctuations are not the primary drive underlying action potentials, we compared subthreshold and suprathreshold responses of the same Dp neurons to different odours (Fig. 3c; $n = 13$ Dp neurons; 6.7 ± 5.5 and 6.7 ± 3.8 subthreshold and suprathreshold trials per neuron, respectively). The magnitude of the slow component was, on average, 10.1 mV larger in suprathreshold responses than in subthreshold responses (15.5 ± 10.7 mV versus 25.6 ± 12.0 mV; $P < 10^{-5}$), whereas the mean amplitude of fluctuations in the 5–40 Hz band was only 0.3 mV larger (0.8 ± 0.5 mV versus 1.1 ± 0.5 mV; $P < 10^{-4}$; Fig. 3c). Hence, oscillatory fluctuations did not substantially contribute to the overall depolarization underlying action potential firing.

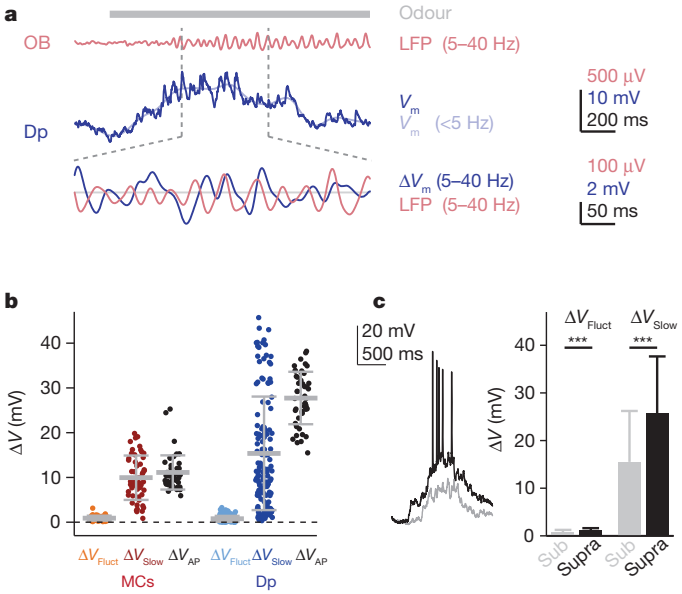

Figure 3 | Spiking responses to odours in Dp are driven by slow depolarization. **a**, Simultaneous recording of LFP in the olfactory bulb (5–40 Hz; red) and membrane potential of a Dp neuron (dark blue) during odour stimulation (grey bar). Light-blue trace shows low-pass (5 Hz) filtered membrane potential. Bottom: comparison of membrane potential fluctuations (difference between original and low-pass filtered membrane potential) and LFP after band-pass-filtering (5–40 Hz) in a 500-ms time window. **b**, Amplitude of membrane potential fluctuations in the oscillatory frequency band (5–40 Hz; ΔV_{Fluct}), amplitude of the slow depolarization (ΔV_{Slow}) in the same trials, and difference between resting potential and spike threshold (ΔV_{AP}) in mitral cells (MCs; left) and Dp neurons (right). Horizontal lines and error bars show mean ± s.d. **c**, Left: subthreshold and suprathreshold responses of a Dp neuron to different odours (Arg, 100 µM, and mixture of Arg and Tyr, 100 µM each). Right: mean amplitude of membrane potential fluctuations (± s.d.) in the oscillatory frequency band (5–40 Hz; ΔV_{Fluct}) and the slow depolarization (ΔV_{Slow}) in subthreshold and suprathreshold responses of the same Dp neurons ($n = 13$). ***$P < 10^{-4}$.

Low-pass filtering mechanisms

To explore why synchrony had no detectable effect on firing rates of Dp neurons we first measured their membrane time constants by step current injections. In randomly selected neurons, time constants were 29 ± 12 ms (mean ± s.d.; $n = 27$ neurons) and 45 ± 18 ms ($n = 30$ neurons) in response to hyperpolarizing and depolarizing steps, respectively (Fig. 4a). In neurons expressing GFP from the promoter of the vesicular glutamate transporter 2a, a marker for glutamatergic neurons, time constants were 67 ± 43 ms and 79 ± 24 ms after hyperpolarizing and depolarizing pulses, respectively ($n = 14$ each; GFP-negative neurons, 33 ± 13 ms and 41 ± 14 ms, $n = 5$ each; $P < 0.01$; Fig. 4a). These time constants are long compared to the temporal precision of spike synchronization in the olfactory bulb[24] and to the period of the oscillation. Passive membrane properties of Dp neurons therefore support low-pass filtering rather than coincidence detection, particularly in glutamatergic neurons.

We then injected sinusoidal currents with fixed or modulated frequencies to examine whether oscillatory input at frequencies near 20 Hz is amplified by active conductances (Supplementary Fig. 12). However, the voltage response decreased gradually as a function of frequency (Fig. 4b), indicating passive low-pass filtering[2]. To examine responses in the spiking regime we simulated synaptic inputs of 20 neurons, each firing at a mean rate of 20 Hz, and varied their oscillatory synchrony by varying S (Supplementary Fig. 4). Simulated spike patterns (10-s duration) were convolved with idealized excitatory postsynaptic current waveforms and injected into Dp neurons in current clamp. The amplitude was adjusted to evoke action potential firing at <10 Hz for $S = 0$. On average, firing rates increased slightly with synchrony, but this effect was not significant (Fig. 4c, d; $P > 0.3$ for all pairwise comparisons). Together, these results indicate that Dp neurons are not intrinsically tuned to detect synchronized input near the natural oscillation frequency but act as passive low-pass filters, unlike Kenyon cells in the mushroom body of insects[9,10,31].

In many brain areas, a delay between excitatory and inhibitory input can establish a narrow time window for the integration of coincident synaptic input[32]. This mechanism selects synchronized input in the insect mushroom body[10] and has been proposed also for olfactory cortex[33–35]. To examine whether delayed inhibition supports coincidence detection in Dp neurons, we recorded excitatory and inhibitory synaptic currents evoked by 20 Hz electrical stimulation of the olfactory tract and analysed synaptic integration in a conductance-based model neuron (Supplementary Fig. 13). Although inhibitory currents were delayed, oscillatory synchrony was not efficiently detected by the model neuron because passive membrane properties act as strong low-pass filters at 20 Hz, and because inhibitory synaptic currents were slow (Supplementary Fig. 13). Our results therefore indicate that slow passive properties, the absence of active amplification, and the slow time course of collective synaptic currents can account, at least in part, for the insensitivity of Dp neurons to synchrony in their inputs.

Late responses of Dp neurons

When responses to optical stimulation were averaged over all neurons, stimuli and synchronizations, the peak of the membrane potential and firing rate responses in Dp ($n = 372$ responses from 34 Dp neurons) occurred approximately 200 ms after the peak of mitral cell responses ($n = 644$ responses from 49 mitral cells; Fig. 5a, b). This effect was

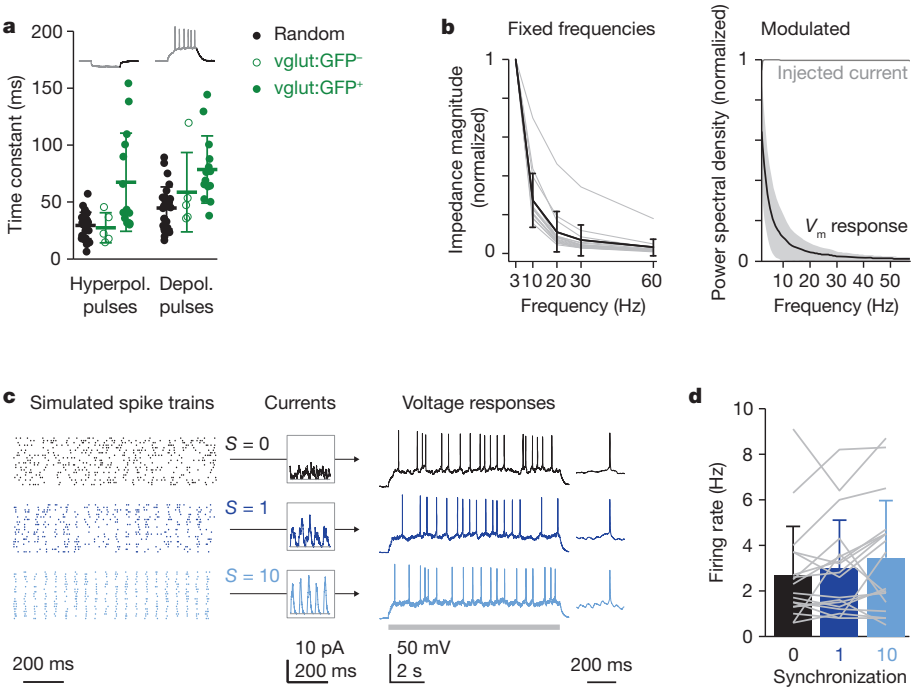

Figure 4 | Intrinsic properties of Dp neurons. **a**, Membrane time constant measured by exponential fits to the membrane potential decay after hyperpolarizing (left) and depolarizing (right) current injection (500 ms). **b**, Normalized impedance of Dp neurons measured by injection of sine currents at five fixed frequencies (left; $n = 15$), and power spectral density of the membrane potential response to injection of frequency-modulated sine currents (right; 1–60 Hz; $n = 9$). Grey traces (left) represent data from individual neurons; grey shading (right) shows s.d. Black traces show mean; error bars show s.d. **c**, Left: examples of simulated spike train patterns. Each row in a spike train pattern shows action potential times of one simulated neuron. Centre: segments of summed currents from spike train patterns with different synchrony. Horizontal grey lines represent zero current. Right: responses of a Dp neuron to currents from spike train patterns with different synchrony. The membrane potential evolution around a single action potential is shown on the right. The grey bar shows time of current injection. **d**, Mean firing frequency (± s.d.) of Dp neurons upon injection of currents from spike train patterns with different synchrony. Grey lines show results from individual cells.

independent of synchrony (compare Figs 1b, e and Figs 1i, l) and also observed when only strong responses (≥10 s.d. of fluctuations before stimulus onset) were considered (Fig. 5c, d). In response to odours, mitral cell firing rates changed during the initial phase of the response and stabilized after approximately 400 ms ($n = 52$ mitral cell–odour pairs; 12 mitral cells in 8 fish), as observed previously[22,24]. Responses of Dp neurons evolved more slowly and peaked substantially later, even when only strong depolarizing responses (≥10 s.d. of pre-odour fluctuations) were considered (Fig. 5e–h and Supplementary Fig. 10). Peak firing of Dp neurons occurred approximately 500 ms later than in mitral cells. Hence, responses of many Dp neurons occurred during the decorrelated steady state of mitral cell activity patterns.

Filtering of oscillatory input and late responses of Dp neurons should favour the detection of decorrelated mitral cell activity patterns. To examine this we measured population activity patterns evoked by three groups of similar amino acid odours (10 μM) using temporally deconvolved two-photon calcium imaging[36]. Odours within each group activate overlapping combinations of glomeruli[37] and evoke mitral cell activity patterns that become decorrelated[22,24,38]. In Dp, correlations between activity patterns were already lower than in the olfactory bulb during the initial phase of the odour response[22,24,38] and subsequently decreased further (Fig. 5i and Supplementary Fig. 14). The transformation of activity patterns between the olfactory bulb and Dp therefore results in decorrelated odour representations, consistent with the temporal filtering properties of Dp neurons.

Discussion

We found that the response intensity of neurons in Dp, a cortex-like target of the olfactory bulb in zebrafish, is largely insensitive to 20 Hz oscillatory synchrony in its input, demonstrating that synchrony does not necessarily enhance responses of target neurons. The impact of synchrony is attenuated because passive properties of Dp neurons and synaptic currents act as low-pass filters. As a consequence, Dp neurons do not directly decode the information contained in the oscillatory synchronization of mitral cell ensembles. However, this information may not be lost because mitral cell synchrony is still reflected in the timing of action potentials in Dp. Moreover, information contained in the synchrony of mitral cell ensembles may be processed by other target areas of the olfactory bulb. Indeed, odour-evoked LFP oscillations phase-locked to those in the olfactory bulb were detected in a distinct area in the central telencephalon (Supplementary Fig. 15).

Many suprathreshold responses of Dp neurons occurred after the peak of the mitral cell response, when mitral cell activity patterns approached their steady state. Multiple mechanisms may contribute to this delay. First, the long membrane time constants of Dp neurons indicate that the integration of synaptic inputs is slow. Second, results from mammalian piriform cortex demonstrated that feed-forward inhibitory neurons are more sensitive to mitral cell input and more broadly tuned than principal neurons[27,34,39,40]. Feed-forward inhibition by a small subset of interneurons may thus suppress responses of other neurons during the early phase of an odour response. Third, inhibitory input to piriform cortex neurons undergoes depression whereas excitatory input undergoes facilitation in response to trains of electrical stimulation in brain slices[39]. These observations are consistent with synaptic currents evoked by olfactory tract stimulation in Dp neurons (Y.-P.Z.S. and R.W.F., unpublished data) and suggest that the net excitatory input increases during later response phases. Fourth, in a recurrent network, the summation of direct and recurrent excitatory input in individual neurons is expected to be maximally effective in the steady state when both inputs are stable. Responses of Dp neurons may therefore be low initially because the network is unable to follow dynamic mitral cell input.

Temporal filtering attenuates the impact of synchronized mitral cell ensembles and early mitral cell activity patterns, which contain

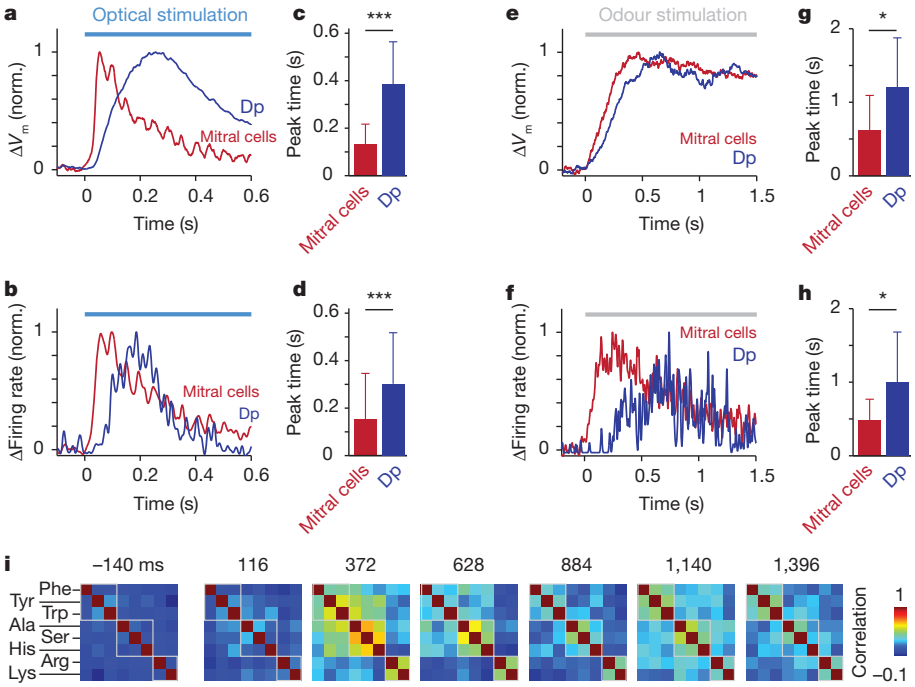

Figure 5 | Late responses of Dp neurons. **a**, Time course of membrane potential responses averaged over all optical stimulus patterns and synchronies (normalized to maximum). Red, mitral cells ($n = 644$ stimulus–neuron pairs in 49 mitral cells); blue, Dp neurons ($n = 372$ stimulus–neuron pairs in 34 Dp neurons). **b**, Average time course of firing rate responses (normalized; same responses). **c**, **d**, Mean time to peak depolarization (± s.d.) of strong membrane potential responses (**c**; ≥10 s.d. of baseline fluctuations; mitral cells, $n = 25$ stimulus–neuron pairs; Dp neurons, $n = 82$) and strong firing rate changes (**d**; mitral cells, $n = 137$; Dp neurons, $n = 58$). **e**, Mean membrane potential time course (normalized) of depolarizing odour responses. Mitral cells and Dp neurons were recorded in the same fish or under the same conditions (mitral cells, $n = 34$ neuron–odour pairs; Dp neurons, $n = 33$). **f**, Mean time course of odour-evoked firing rate responses (normalized). **g**, **h**, Mean time-to-peak (± s.d.) of strong depolarizing responses (**g**; ≥10 s.d.; mitral cells, $n = 12$; Dp neurons, $n = 14$) and strong firing rate responses to odours (**h**; ≥10 s.d.; mitral cells, $n = 15$; Dp neurons, $n = 19$). $*P < 0.05$; $***P < 10^{-9}$. **i**, Pearson correlation between activity patterns ($n = 405$ neurons from 5 fish) evoked by different odours as a function of time. Activity patterns were measured using temporally deconvolved two-photon calcium imaging. Time relative to stimulus onset ($t = 0$) is shown above each correlation matrix in milliseconds. Left correlation matrix ($t = -140$ ms) shows pre-stimulus correlations.

information about molecular categories but are not well suited for fine odour discrimination. Temporal filtering therefore tunes Dp neurons to features of mitral cell responses that are particularly informative about precise odour identity. Consistent with these filtering operations, activity patterns evoked by similar odours were more distinct in Dp than in the olfactory bulb. The transformation between the olfactory bulb and Dp therefore establishes specific and decorrelated odour representations, which is a prerequisite for higher-order computations such as pattern storage by auto-associative networks.

Contrary to neurons in Dp, Kenyon cells in the insect mushroom body are exquisitely sensitive to oscillatory synchronization[10,41] and respond preferentially during the initial phase of an odour response[9,25]. Pattern read out in the mushroom body is therefore different from Dp. However, odour representations differ already at the previous processing stage: in the antennal lobe, response patterns are dense, synchronized ensembles represent odour identity, and the dynamic phase of the odour response is more informative than the steady state[6,25]. Moreover, the convergence onto second-order neurons in the insect mushroom body is high[42], unlike in olfactory cortex[27]. Under these conditions, the detection of synchronized ensembles results in highly selective, robust and sparse odour representations[9,10,41]. Second-order processing therefore extracts information about precise odour identity both in zebrafish and insects. In zebrafish, temporal constraints on odour processing may be less strict than in other species because zebrafish live in non-turbulent environments and do not sniff[43,44]. As a consequence, zebrafish may afford to use steady-state activity patterns for neuronal computations. In general, our results show that temporal filters can be tuned to extract specific information from multiplexed neuronal codes, indicating that multiplexing can be used by the brain to efficiently encode and transmit information.

METHODS SUMMARY

Experiments were performed in an explant preparation of the intact brain and nose of adult zebrafish[22]. Odour stimulation, electrophysiological recordings and temporally deconvolved calcium imaging were performed as described[22,26,36]. Chr2 was expressed in sensory afferents under the control of the Tet system as described[30] or, in a few fish, using the promoter of olfactory marker protein[45]. Spatio-temporal patterns of blue laser light were projected onto the olfactory bulb through the objective of an upright microscope using a DMD with an accelerator board (DMD Discovery 1100 with ALP-1; Texas Instruments) that enabled temporal resolution up to 0.125 ms.

Full Methods and any associated references are available in the online version of the paper at www.nature.com/nature.

Received 17 May; accepted 13 October 2011.
Published online 13 November 2011.

1. Gerstner, W., Kreiter, A. K., Markram, H. & Herz, A. V. Neural codes: firing rates and beyond. *Proc. Natl Acad. Sci. USA* **94,** 12740–12741 (1997).
2. Hutcheon, B. & Yarom, Y. Resonance, oscillation and the intrinsic frequency preferences of neurons. *Trends Neurosci.* **23,** 216–222 (2000).
3. Fries, P. Neuronal gamma-band synchronization as a fundamental process in cortical computation. *Annu. Rev. Neurosci.* **32,** 209–224 (2009).
4. Gütig, R. & Sompolinsky, H. The tempotron: a neuron that learns spike timing-based decisions. *Nature Neurosci.* **9,** 420–428 (2006).
5. Laurent, G. Olfactory network dynamics and the coding of multidimensional signals. *Nature Rev. Neurosci.* **3,** 884–895 (2002).
6. Rabinovich, M., Huerta, R. & Laurent, G. Transient dynamics for neural processing. *Science* **321,** 48–50 (2008).
7. Buzsaki, G. & Draguhn, A. Neuronal oscillations in cortical networks. *Science* **304,** 1926–1929 (2004).

8. Singer, W. Neuronal synchrony: a versatile code for the definition of relations? *Neuron* **24,** 49–65 (1999).
9. Perez-Orive, J., Bazhenov, M. & Laurent, G. Intrinsic and circuit properties favor coincidence detection for decoding oscillatory input. *J. Neurosci.* **24,** 6037–6047 (2004).
10. Perez-Orive, J. *et al.* Oscillations and sparsening of odor representations in the mushroom body. *Science* **297,** 359–365 (2002).
11. Azouz, R. & Gray, C. M. Adaptive coincidence detection and dynamic gain control in visual cortical neurons *in vivo*. *Neuron* **37,** 513–523 (2003).
12. Bruno, R. M. & Sakmann, B. Cortex is driven by weak but synchronously active thalamocortical synapses. *Science* **312,** 1622–1627 (2006).
13. Gawne, T. J., Kjaer, T. W. & Richmond, B. J. Latency: another potential code for feature binding in striate cortex. *J. Neurophysiol.* **76,** 1356–1360 (1996).
14. Hopfield, J. J. Pattern recognition computation using action potential timing for stimulus representation. *Nature* **376,** 33–36 (1995).
15. Gollisch, T. & Meister, M. Rapid neural coding in the retina with relative spike latencies. *Science* **319,** 1108–1111 (2008).
16. Junek, S., Kludt, E., Wolf, F. & Schild, D. Olfactory Coding with Patterns of Response Latencies. *Neuron* **67,** 872–884 (2010).
17. Spors, H., Wachowiak, M., Cohen, L. B. & Friedrich, R. W. Temporal dynamics and latency patterns of receptor neuron input to the olfactory bulb. *J. Neurosci.* **26,** 1247–1259 (2006).
18. Bathellier, B., Buhl, D. L., Accolla, R. & Carleton, A. Dynamic ensemble odor coding in the mammalian olfactory bulb: sensory information at different timescales. *Neuron* **57,** 586–598 (2008).
19. Cury, K. M. & Uchida, N. Robust odor coding via inhalation-coupled transient activity in the mammalian olfactory bulb. *Neuron* **68,** 570–585 (2010).
20. Maass, W., Natschlager, T. & Markram, H. Real-time computing without stable states: a new framework for neural computation based on perturbations. *Neural Comput.* **14,** 2531–2560 (2002).
21. Sugase, Y., Yamane, S., Ueno, S. & Kawano, K. Global and fine information coded by single neurons in the temporal visual cortex. *Nature* **400,** 869–873 (1999).
22. Friedrich, R. W. & Laurent, G. Dynamic optimization of odor representations in the olfactory bulb by slow temporal patterning of mitral cell activity. *Science* **291,** 889–894 (2001).
23. Ringach, D. L., Hawken, M. J. & Shapley, R. Dynamics of orientation tuning in macaque primary visual cortex. *Nature* **387,** 281–284 (1997).
24. Friedrich, R. W., Habermann, C. J. & Laurent, G. Multiplexing using synchrony in the zebrafish olfactory bulb. *Nature Neurosci.* **7,** 862–871 (2004).
25. Mazor, O. & Laurent, G. Transient dynamics versus fixed points in odor representations by locust antennal lobe projection neurons. *Neuron* **48,** 661–673 (2005).
26. Yaksi, E., von Saint Paul, F., Niessing, J., Bundschuh, S. T. & Friedrich, R. W. Transformation of odor representations in target areas of the olfactory bulb. *Nature Neurosci.* **12,** 474–482 (2009).
27. Miyamichi, K. *et al.* Cortical representations of olfactory input by trans-synaptic tracing. *Nature* **472,** 191–196 (2011).
28. Nagel, G. *et al.* Channelrhodopsin-2, a directly light-gated cation-selective membrane channel. *Proc. Natl Acad. Sci. USA* **100,** 13940–13945 (2003).
29. Boyden, E. S., Zhang, F., Bamberg, E., Nagel, G. & Deisseroth, K. Millisecond-timescale, genetically targeted optical control of neural activity. *Nature Neurosci.* **8,** 1263–1268 (2005).
30. Zhu, P. *et al.* Optogenetic dissection of neuronal circuits in zebrafish using viral gene transfer and the Tet system. *Front. Neural Circuits* **3,** 21 (2009).
31. Laurent, G. & Naraghi, M. Odorant-induced oscillations in the mushroom bodies of the locust. *J. Neurosci.* **14,** 2993–3004 (1994).
32. Pouille, F. & Scanziani, M. Enforcement of temporal fidelity in pyramidal cells by somatic feed-forward inhibition. *Science* **293,** 1159–1163 (2001).
33. Franks, K. M. & Isaacson, J. S. Strong single-fiber sensory inputs to olfactory cortex: implications for olfactory coding. *Neuron* **49,** 357–363 (2006).
34. Luna, V. M. & Schoppa, N. E. GABAergic circuits control input-spike coupling in the piriform cortex. *J. Neurosci.* **28,** 8851–8859 (2008).
35. Ketchum, K. L. & Haberly, L. B. Synaptic events that generate fast oscillations in piriform cortex. *J. Neurosci.* **13,** 3980–3985 (1993).
36. Yaksi, E. & Friedrich, R. W. Reconstruction of firing rate changes across neuronal populations by temporally deconvolved Ca^{2+} imaging. *Nature Methods* **3,** 377–383 (2006).
37. Friedrich, R. W. & Korsching, S. I. Combinatorial and chemotopic odorant coding in the zebrafish olfactory bulb visualized by optical imaging. *Neuron* **18,** 737–752 (1997).
38. Niessing, J. & Friedrich, R. W. Olfactory pattern classification by discrete neuronal network states. *Nature* **465,** 47–52 (2010).
39. Stokes, C. C. & Isaacson, J. S. From dendrite to soma: dynamic routing of inhibition by complementary interneuron microcircuits in olfactory cortex. *Neuron* **67,** 452–465 (2010).
40. Poo, C. & Isaacson, J. S. Odor representations in olfactory cortex: ''sparse'' coding, global inhibition, and oscillations. *Neuron* **62,** 850–861 (2009).
41. Stopfer, M., Jayaraman, V. & Laurent, G. Intensity versus identity coding in an olfactory system. *Neuron* **39,** 991–1004 (2003).
42. Jortner, R. A., Farivar, S. S. & Laurent, G. A simple connectivity scheme for sparse coding in an olfactory system. *J. Neurosci.* **27,** 1659–1669 (2007).
43. Spence, R., Gerlach, G., Lawrence, C. & Smith, C. The behaviour and ecology of the zebrafish, *Danio rerio*. *Biol. Rev. Camb. Philos. Soc.* **83,** 13–34 (2008).
44. Engeszer, R. E., Patterson, L. B., Rao, A. A. & Parichy, D. M. Zebrafish in the wild: a review of natural history and new notes from the field. *Zebrafish* **4,** 21–40 (2007).
45. Sato, Y., Miyasaka, N. & Yoshihara, Y. Mutually exclusive glomerular innervation by two distinct types of olfactory sensory neurons revealed in transgenic zebrafish. *J. Neurosci.* **25,** 4889–4897 (2005).

Supplementary Information is linked to the online version of the paper at www.nature.com/nature.

Acknowledgements This work was supported by the Novartis Research Foundation, the Max-Planck-Society, the Swiss National Fonds (SNF), the Deutsche Forschungsgemeinschaft (DFG), the Human Frontier Science Program (HFSP), and the Whitaker Foundation (J.S.). We are grateful to S.-i. Higashijima for vglut2a-GFP transgenic fish and thank T. Frank, A. Lüthi, I. Namekawa and T. Oertner for comments on the manuscript.

Author Contributions F.B. performed electrophysiological experiments, analysed data and wrote part of the manuscript. P.Z. generated transgenic fish, participated in the construction of the DMD device, performed optogenetic experiments, recorded LFPs and analysed data. J.S. constructed the DMD device and performed optogenetic experiments. Y.-P.Z.S. performed electrophysiological experiments, participated in the construction of the DMD device, performed calcium imaging experiments, recorded LFPs and analysed data. E.Y. participated in calcium imaging experiments. K.D. contributed channelrhodopsin-2 constructs. R.W.F. conceived the study, designed equipment, analysed data, performed modelling and wrote the manuscript.

Author Information Reprints and permissions information is available at www.nature.com/reprints. The authors declare no competing financial interests. Readers are welcome to comment on the online version of this article at www.nature.com/nature. Correspondence and requests for materials should be addressed to R.W.F. (Rainer.Friedrich@fmi.ch).

METHODS

Animals, experimental preparation and odour delivery. Experiments were performed in adult zebrafish (*Danio rerio*) that were raised and kept under standard laboratory conditions (26.5 °C; 13/11-h light/dark cycle). All experiments were performed in accordance with official guidelines and approved by the Veterinary Department of the Canton Basel-Stadt (Switzerland). For optical stimulation of sensory inputs to the olfactory bulb, transgenic fish lines were used that express Chr2 (refs 28, 29) selectively in sensory afferents to the olfactory bulb. Five out of thirty-four transgenic fish expressed Chr2 under a 2-kb fragment of the promoter of the zebrafish olfactory marker protein gene[45]. This line expresses Chr2 mainly in sensory afferents projecting to the medial and dorsal olfactory bulb, as described for other transgenic lines generated with this promoter[45]. Fish used in the remaining 29 experiments were generated by expressing Chr2 under the control of a HuC promoter fragment[46] using the Tet system[47], which results in diverse expression patterns in different founder lines[30]. For experiments in this study, one line was selected that expressed Chr2 in the olfactory bulb selectively in sensory afferents without any obvious regional bias (HuC:itTA/Ptet:Chr2YFP Line 02)[30]. Experiments not including Chr2 stimulation were performed in wild-type fish or fish[48] expressing green fluorescent protein under the control of a promoter of the vesicular glutamate transporter 2a.

Fish were cold-anaesthetized, decapitated and the ventral forebrain was exposed by removal of the jaws and palate. The preparation was transferred into a custom chamber, continuously superfused with teleost artificial cerebrospinal fluid (ACSF)[49], and warmed up to room temperature. Odours were introduced into a constant stream directed at one naris using a computer-controlled HPLC injection valve. Odour stimuli took approximately 600 ms to reach a plateau concentration and lasted approximately 2.5 s in total. Odour applications were separated in time by at least 40 s, usually longer, to minimize adaptation. Each odour was applied, on average, 4.1 ± 1.8 (mean ± s.d.) times and results were averaged, except for the analysis of membrane potential fluctuations and their relationship to LFP oscillations in individual trials, and for power spectral analysis.

Electrophysiological recordings, calcium imaging and tract stimulation. Whole-cell patch-clamp recordings were performed using borosilicate pipettes filled with intracellular solution containing (in mM): 130 K-gluconate, 10 Na-gluconate, 10 Na-phosphocreatine, 4 NaCl, 4 Mg-ATP, 0.3 Na-GTP, 10 HEPES (pH 7.25; ~300 mosM). For voltage clamp recordings, a Cs-based internal solution was used that contained (in mM): 135 Cs-methanesulphonate, 3 Na-ascorbate, 10 Na-phosphocreatine, 4 $MgCl_2$, 4 Na_2-ATP, 0.4 Na-GTP, 10 HEPES (pH 7.2; 300 mosM). In most experiments, pipette solutions also contained the fluorescent dye Alexa594 to visualize neuronal morphology under two-photon optics. Pipettes had resistances of 10–16 MΩ and were targeted to somata using contrast-enhanced optics that detected the transmitted infrared laser beam in a two-photon microscope. Signals were recorded at 10 kHz using a Multiclamp 700B amplifier (Molecular Devices) and Scanimage/Ephus software[50,51]. Recording stability was assessed regularly by test pulses. All recorded neurons responded to current injection with action potentials. LFPs were recorded using glass pipettes filled with ACSF and a Multiclamp 700B amplifier.

To stimulate olfactory tracts, glass pipettes filled with ACSF were placed at individual fibre bundles. Because olfactory tracts in zebrafish consist of many dispersed fibre bundles, only a small subset of axons was stimulated by this approach. Stimuli consisted of 10 pulses of 0.5 ms duration at 20 Hz. Intensity (usually 20–30 V) was adjusted to evoke a response of intermediate magnitude.

Multiphoton calcium imaging of odour responses was performed as described[26,36]. Data were acquired at 128 ms per frame. Relative firing rate changes were reconstructed from calcium signals by low-pass filtering and subsequent temporal deconvolution with an exponentially decaying kernel as described[36]. The decay time constant of the kernel (τ_{decay} = 3 s) was determined by simultaneous calcium imaging and loose-patch recordings of spikes[36]. No additional filtering before or after deconvolution was performed.

Optical stimulation. To generate spatio-temporal patterns of light, the beam of a blue laser (500 mW) was expanded to match the minor diameter (10.5 mm) of a digital micromirror device (DMD) equipped with an accelerator card that allowed for switching each mirror between two angles with a temporal resolution up to 0.125 ms (DMD Discovery 1100 with ALP-1; Texas Instruments). The device was coupled into a two-photon laser scanning microscope using a custom lens system and a dichroic mirror at 45° between the scanners and scan lens. The DMD device was mounted so that the laser light reflected from a given mirror either entered the microscope optics ('on' angle) or was deflected into a beam dump ('off' angle). Light patterns entering the microscope were projected into the image plane through the scan lens, the tube lens, and the objective (20×, NA 1.0, Zeiss). Each mirror of the DMD corresponded to a 0.67 × 0.67 μm^2 pixel in the image plane. Light intensity below the objective was 63 $\mu W\,mm^{-2}$. To verify proper resolution, light patterns were projected onto a thin film of fluorescein solution and fluorescence images were collected using a CCD camera (Supplementary Fig. 2).

Optical stimulation of mitral cells was performed by projecting spatio-temporal patterns of blue light onto the olfactory bulb in fish expressing Chr2 in sensory afferents. In each stimulus, a subset of 'active' squares was switched on and off in a temporal sequence determined by event trains (see below), whereas 'inactive' squares remained off. Two sets of spatial stimulus patterns were generated. Stimulus set 1 consisted of 50 × 50 μm^2 squares in the image plane (75 × 75 mirrors). Mirrors within each square were switched on and off together, while different squares were controlled by different event trains. Stimulus set 2 consisted of 20 × 20 μm^2 squares (30 × 30 mirrors), and each mirror was controlled by an individual event train. At each event in a train, the corresponding square (set 1) or mirror (set 2) was switched from the 'off' to the 'on' position for 5 ms to deliver a pulse of blue light to the corresponding pixels in the image plane. The average event rate for each square or mirror was zero before and after the optical stimulus and 20 Hz during stimulation. In set 2, random latencies between zero and 300 ms were assigned to each square to mimic latency differences between responses of different glomeruli. The synchrony between event trains controlling different squares or mirrors was defined by the synchronization index S (see below). Spatial patterns were created with active squares only over the lateral olfactory bulb, over the medial olfactory bulb, or over the whole olfactory bulb (Supplementary Fig. 2). On average, each optical stimulus was repeated 3.4 ± 1.2 times (mean ± s.d.; mitral cells, 3.4 ± 1.1 repetitions; Dp neurons, 3.5 ± 1.2 repetitions) and results were averaged (except for power spectral analysis).

Responses to stimulus set 2 (n = 68 responses from 21 mitral cells and n = 55 responses from 18 Dp neurons at each S) increased more slowly than responses to stimulus set 1 (n = 93 responses from 28 mitral cells and n = 38 responses from 16 Dp neurons) because squares were activated successively during the initial 300 ms. However, the time difference between responses of mitral cell and Dp neurons was similar in response to both stimulus sets: the mean peak time of strong depolarizations (>10 s.d.) in response to stimulus set 1 was 108 ± 48 ms for mitral cells and 263 ± 110 ms for Dp neurons. The mean peak time of strong depolarizations (>10 s.d.) in response to stimulus set 2 was 261 ± 125 ms for mitral cells and 438 ± 178 ms for Dp neurons. The mean peak time of strong firing rate changes (>10 s.d.) in response to stimulus set 1 was 132 ± 179 ms for mitral cells and 283 ± 213 ms for Dp neurons. The mean peak time of strong firing rate changes (>10 s.d.) in response to stimulus set 2 was 267 ± 228 ms for mitral cells and 407 ± 206 ms for Dp neurons. Otherwise, responses to both stimulus sets were similar. Data obtained with the two stimulus sets were therefore pooled.

The stability of mitral cell firing rates to changes in synchrony may be due to the fact that mitral cell membrane potentials are near spike threshold already in the absence of odour stimulation so that synchrony affects primarily the timing of action potentials. Moreover, stronger mitral cell activation is counterbalanced by increased feedback inhibition in the olfactory bulb[52], and inputs of different strengths might be equalized by a nonlinear transformation at the sensory neuron-to-mitral cell synapse, as found in *Drosophila*[53].

Generation of event trains and modelling. To generate trains of events (spike times or DMD mirror activations) with varying degrees of synchrony, individual events were drawn from probability distribution $P(t)$ given by

$$P(t) = X(t) / \int_0^{t_{max}} X(t)\mathrm{d}t \text{ with}$$

$$X(t) = (S \times \sin(20 \times 2\pi \times t) + 1) \quad | S \le 1$$

$$X(t) = (\sin(20 \times 2\pi \times t) + 1)^S \quad | S \le 1$$

where $t \le t_{max}$ is time in seconds and S is the synchronization index. To allow for a refractory period, events closer than 5 ms to an event kept previously were discarded. This procedure was repeated until the mean number of events per unit time was equal to the desired event rate. For S = 0, the instantaneous probability of an event was defined to be constant. This procedure parameterized synchrony in simulated spike trains and in optical stimulus patterns.

Event trains were transformed into excitatory postsynaptic currents by convolving the delta functions representing event times with an alpha function representing a unitary excitatory postsynaptic current (EPSC; rise time, 0.8 ms; decay time, 5 ms).

To simulate the integration of synaptic currents in a simple model, a conductance-based, non-spiking point neuron model without voltage-gated conductances was used. The input resistance R_{in} was 2 GΩ and the time constant was τ_m = 40 ms, similar to values measured in Dp neurons. The neuron received n = 10 inputs, each firing at a mean rate of 10 Hz. Each input spike evoked excitatory and inhibitory synaptic currents with a time course (250 ms length) given by the mean current measured at these potentials in Dp neurons in response to electrical stimulation of the olfactory tract (Supplementary Fig. 13). Since time courses of

synaptic currents could be measured only over 50 ms between successive stimulus pulses, the remaining 200 ms were extrapolated by exponential functions. Reversal potentials of excitatory and inhibitory synaptic currents were $V_{rev,exc} = 0$ mV and $V_{rev,inh} = -70$ mV, respectively. The evolution of the membrane potential V_m was then given by

$$C dV_m/dt = -g_0(V(t) - V_{rev,0}) - g_{exc}(t)\,(V(t) - V_{rev,exc}) - g_{inh}(t)\,(V(t) - V_{rev,inh})$$

where $C = \tau_m/R_{in}$ is membrane capacitance, $g_0 = 1/R_{in}$ is the input conductance, $V_{rev,0} = -70$ mV is the resting potential, $g_{exc}(t)$ is the excitatory synaptic conductance and $g_{inh}(t)$ is the inhibitory synaptic conductance.

Simulations were performed for input spike patterns with three different synchronies *S*. For each synchrony, we also shifted the onset of inhibitory currents backward and forward in time (−5 ms and +20 ms). Moreover, we varied the mean firing rate of each input between 8 Hz and 12 Hz, and the number of inputs *N* between 8 and 12 (without changing the amplitude of synaptic currents). For each condition, results of 128 simulations, each 2.5 s long, were averaged.

Data analysis. Power spectral analysis was performed on individual trials. Power spectra were then first averaged over trials with the same stimulus, and subsequently averaged over stimulus–neuron pairs. LFPs in the olfactory bulb were recorded in the deep layers, beyond the point of reversal[24]. Oscillations were analysed by band-pass filtering LFP recordings between 5 and 40 Hz using a non-causal filter designed in Matlab (The MathWorks). Spike phases were determined by the time of each spike relative to the neighbouring peaks in the band-pass filtered LFP. Spike phase distributions were determined for each neuron–stimulus pair from repeated trials and normalized by the number of trials and spikes. Experiments in which less than 16 spikes were collected in total were excluded. Distributions were then averaged over neuron–stimulus pairs.

Trains of action potentials were transformed into continuous firing rates by convolution with a Gaussian kernel (s.d., 5 ms). Mean changes in membrane potential and mean firing rates in response to optical stimulation were determined within a 1-s time window following stimulus onset. For analyses of membrane potential dynamics, action potentials were removed by a sliding median filter with width 14 ms. To determine peak times of membrane potential responses, the time course of the median-filtered membrane potential trace was smoothed by a non-causal four-pole low-pass Butterworth filter with cutoff frequency 50 Hz.

The resting potential was determined as the mean over the 500 lowest membrane potential values (1-ms bins) during a 1.5–3 s pre-odour period. Action potential thresholds were determined as the inflection point of action potentials in each trial. To determine the amplitude of membrane potential fluctuations in the 5–40 Hz band and of the slow depolarization during odour stimulation, membrane potential traces were first low-pass filtered by a non-causal four-pole Butterworth filter with cutoff frequency 5 Hz. The amplitude of the slow depolarization was quantified as the difference between the resting potential and the peak of the low-pass filtered membrane potential trace. Fluctuations were isolated by subtracting the low-pass filtered trace from the raw trace and subsequently band-pass filtered with the same filter as used for the LFP. The amplitudes of fluctuations were then quantified as the amplitudes of the positive peaks. Maximal amplitudes of fluctuations in a given trial were determined as the mean over the 10% largest fluctuations. For the separate analysis of subthreshold and suprathreshold responses, subthreshold responses were defined as neuron–stimulus pairs that never responded with action potentials to a given odour, whereas suprathreshold responses were defined as responses that included, on average, at least one spike.

Significance tests were performed using a non-parametric Wilcoxon rank-sum test unless noted otherwise.

46. Higashijima, S., Masino, M. A., Mandel, G. & Fetcho, J. R. Imaging neuronal activity during zebrafish behavior with a genetically encoded calcium indicator. *J. Neurophysiol.* **90,** 3986–3997 (2003).
47. Gossen, M. & Bujard, H. Tight control of gene expression in mammalian cells by tetracycline-responsive promoters. *Proc. Natl Acad. Sci. USA* **89,** 5547–5551 (1992).
48. Miyasaka, N. *et al.* From the olfactory bulb to higher brain centers: genetic visualization of secondary olfactory pathways in zebrafish. *J. Neurosci.* **29,** 4756–4767 (2009).
49. Mathieson, W. B. & Maler, L. Morphological and electrophysiological properties of a novel in vitro preparation: the electrosensory lateral line lobe brain slice. *J. Comp. Physiol. A* **163,** 489–506 (1988).
50. Pologruto, T. A., Sabatini, B. L. & Svoboda, K. ScanImage: flexible software for operating laser scanning microscopes. *Biomed. Eng. Online* **2,** 13 (2003).
51. Suter, B. A. *et al.* Ephus: multipurpose data acquisition software for neuroscience experiments. *Front. Neural Circuits* **4,** 100 (2010).
52. Tabor, R. & Friedrich, R. W. Pharmacological analysis of ionotropic glutamate receptor function in neuronal circuits of the zebrafish olfactory bulb. *PLoS ONE* **3,** e1416 (2008).
53. Bhandawat, V., Olsen, S. R., Gouwens, N. W., Schlief, M. L. & Wilson, R. I. Sensory processing in the *Drosophila* antennal lobe increases reliability and separability of ensemble odor representations. *Nature Neurosci.* **10,** 1474–1482 (2007).